Hindawi
Wireless Communications and Mobile Computing
Volume 2020, Article ID 6698446, 12 pages
https://doi.org/10.1155/2020/6698446

Research Article

An Accurate Sparse Recovery Algorithm for Range-Angle Localization of Targets via Double-Pulse FDA-MIMO Radar

Qi Liu,[1] **Xianpeng Wang**,[1] **Liangtian Wan**,[2] **Mengxing Huang**,[1] **and Lu Sun**[3]

[1]*State Key Laboratory of Marine Resource Utilization in South China Sea and School of Information and Communication Engineering, Hainan University, Haikou 570228, China*
[2]*Key Laboratory for Ubiquitous Network and Service Software of Liaoning Province, School of Software, Dalian University of Technology, Dalian 116620, China*
[3]*Department of Communication Engineering, Institute of Information Science Technology, Dalian Maritime University, 116026, China*

Correspondence should be addressed to Xianpeng Wang; wxpeng2016@hainu.edu.cn

Received 17 October 2020; Revised 16 November 2020; Accepted 29 November 2020; Published 16 December 2020

Academic Editor: Lisheng Fan

In this paper, a sparse recovery algorithm based on a double-pulse FDA-MIMO radar is proposed to jointly extract the angle and range estimates of targets. Firstly, the angle estimates of targets are calculated by transmitting a pulse with a zero frequency increment and employing the improved l_1-SVD method. Subsequently, the range estimates of targets are achieved by utilizing a pulse with a nonzero frequency increment. Specifically, after obtaining the angle estimates of targets, we perform dimensionality reduction processing on the overcomplete dictionary to achieve the automatically paired range and angle in range estimation. Grid partition will bring a heavy computational burden. Therefore, we adopt an iterative grid refinement method to alleviate the above limitation on parameter estimation and propose a new iteration criterion to improve the error between real parameters and their estimates to get a trade-off between the high-precision grid and the atomic correlation. Finally, the proposed algorithm is evaluated by providing the results of the Cramér-Rao lower bound (CRLB) and numerical root mean square error (RMSE).

1. Introduction

Target localization has been acting as a pivotal part in the field of array signal processing, which expects various applications in radar, navigation, and communication [1–4]. In recent years, multiple-input multiple-output (MIMO) radar [5, 6] has attracted widespread consideration in target localization due to many potential merits [7], where multiple antennas are utilized to transmit different waveforms at the same time and simultaneously receive reflected signals. Compared with the phased array radar, MIMO radar can obtain enhanced spatial resolution, improved estimation performance, and increased degrees of freedom (DOF) [8–10] by effectively utilizing space diversity. However, MIMO radar cannot obtain the essential range estimates of targets. FDA-MIMO [11–14] radar, as a combination of frequency diverse array (FDA) radar [15–17] and MIMO radar, has a small frequency increment in adjacent transmitting array antennas to achieve the joint estimation of the angle and range [18].

Nowadays, the traditional DOA estimation algorithms have been applied for the joint angle-range estimation of FDA-MIMO radar, such as the estimation of signal parameters via rotational invariance techniques (ESPRIT) [19], unitary ESPRIT (U-ESPRIT) [20], and two-dimensional multiple signal classification (2D-MUSIC) [21]. However, the aforementioned algorithms based on subspace decomposition usually require a large number of snapshots and encounter performance degradation in the case of highly correlated targets.

The compressed sensing technique has attracted extensive attention in sparse signal reconstruction to deal with the above limitation of the subspace-based algorithms. The sparse signal recovery (SSR) algorithms [22–24] mainly estimate target parameters by constructing a sparse signal model and reconstructing the spatial spectrum. In an environment

with a low signal-to-noise ratio (SNR) or a small number of snapshots, the SSR algorithm outperforms the subspace-based method in parameter estimation performance [25, 26]. In the past several years, some SSR algorithms have been presented, such as the sparse Bayesian learning (SBL) algorithm [27, 28], l_1-norm singular value decomposition (SVD) algorithm [29], and l_1-norm sparse representation of array covariance vector (SRACV) algorithm [30]. Nevertheless, they suffer from a complex two-dimensional overcomplete dictionary, which will bring a heavy computational burden.

In this paper, a sparse recovery algorithm is proposed based on a double-pulse FDA-MIMO radar. We extend the double-pulse concept of FDA radar in [31] to FDA-MIMO radar to solve the high-complexity problem of sparse recovery algorithms and simultaneously improve the parameter estimation performance of FDA-MIMO radar. Firstly, the angle estimates of targets are calculated by utilizing a pulse with a zero frequency increment and employing the improved l_1-SVD method. Subsequently, the range estimates of targets are achieved by transmitting a pulse with a nonzero frequency increment. Specifically, after obtaining the angle estimates of targets, we deleted the unnecessary elements in the overcomplete dictionary to reduce its dimensionality during the range estimation. Therefore, this algorithm not only decouples the angle and range of FDA-MIMO radar but also reduces the dimension of the overcomplete dictionary. Grid partition will bring the problem of the heavy computational burden. As a result, we utilize an iterative grid refinement method to overcome the adverse effects caused by the grid partition on parameter estimation. Furthermore, we propose a new iteration criterion to improve the error between real parameters and their estimates to get a trade-off between the high-precision grid and the atomic correlation, so the proposed algorithm can achieve better target localization performance with FDA-MIMO radar as compared with the subspace-based algorithm. Finally, we derive the CRLB for the target parameter of the double-pulse FDA-MIMO radar. Numerical simulation verifies the superior performance of the proposed algorithm.

Notation. Capital bold letters and lowercase bold letters represent matrices and vectors, respectively. $(\cdot)^*$, $(\cdot)^{-1}$, and $(\cdot)^T$ stand for conjugate, inverse, and transpose operations, respectively. $\odot$ represents the Hadamard product, and $\otimes$ denotes the Kronecker product. $\|\bullet\|_1$ and $\|\bullet\|_2$ denote l_1-norm and l_2-norm, respectively. $\mathbb{C}^{P\times Q}$ denotes a $P \times Q$ complex matrix set.

2. Signal Model

As shown in Figure 1, a monostatic double-pulse FDA-MIMO radar that consists of uniform linear arrays (ULAs) with interelement spacing $d = \lambda/2$ is considered, where the transmitter has M antennas and the receiver has N antennas. The first antenna in the transmitter is treated as the reference point. Considering the linearly increasing frequency increments, the carrier frequency at the m-th transmitter antenna is

$$f_m = f_1 + (m-1)\Delta f, \quad m = 1, 2, \cdots, M, \tag{1}$$

where Δf denotes the frequency increment and f_1 stands for the carrier frequency of the first antenna in the transmitter, where $\Delta f \ll f_1$.

Suppose the narrowband signal emitted by the m-th antenna is

$$s_m(t) = \phi_m(t) e^{j2\pi f_m t}, \quad m = 1, 2, \cdots, M, 0 \le t \le T, \tag{2}$$

where T is the duration of the radar pulse and $\phi_m(t)$ is the m-th baseband waveform which follows that

$$\int_0^T \phi_m(t)\phi_n^*(t-\tau)e^{j2\pi(m-n)\Delta f t}dt = \begin{cases} 1, & m = n, \tau = 0, \\ 0, & m \ne n, \forall \tau, \end{cases} \tag{3}$$

where τ represents the time delay.

Assume that there are K far-field targets in the far-field whose ranges are much larger than the aperture of FDA-MIMO radar. Subsequently, the signal received by the n-th antenna in the receiver and transmitted by the m-th antenna in the transmitter can be represented by

$$x_{m,n}(t) = \sum_{k=1}^{K} \phi_m(t - \tau(m, n, \theta_k, r_k)) e^{j2\pi f_m (t - \tau(m,n,\theta_k,r_k))}, \tag{4}$$

where $\tau(m, n, \theta_k, r_k)$ represents the delay between the m-th antenna in the transmitter and the n-th antenna in the receiver, which is expressed as

$$\tau(m, n, \theta_k, r_k) = \frac{2r_k}{c} - \frac{(m-1)d_t \sin(\theta_k)}{c} - \frac{(n-1)d_r \sin(\theta_k)}{c}, \tag{5}$$

where r_k and θ_k are the range and angle of the k-th target. d_t and d_r are the interval between transmitter antennas and receiver antennas, respectively. c is the speed of light.

The outputs of the received data after the matched filter (MF) can be expressed as [14]

$$\mathbf{x}(l) = \mathbf{A}\mathbf{s}(l) + \mathbf{n}(l), \tag{6}$$

where $\mathbf{s}(l) = [s_1(l), s_2(l), \cdots, s_K(l)]^T \in \mathbb{C}^{K\times 1}$ is a signal vector. $\mathbf{n}(l)$ represents the noise vector. $\mathbf{A} = [\bar{\mathbf{a}}(\theta_1, r_1), \bar{\mathbf{a}}(\theta_2, r_2), \cdots, \bar{\mathbf{a}}(\theta_K, r_K)] \in \mathbb{C}^{MN\times K}$ is a joint steering vector matrix, and $\bar{\mathbf{a}}(\theta_k, r_k) = \mathbf{a}_r(\theta_k) \otimes \mathbf{a}_t(\theta_k, r_k)$ with $k = 1, 2, \cdots, K$. The steering vectors of the receiver and transmitter can be defined by [13]

$$\begin{aligned} \mathbf{a}_r(\theta_k) &= \left[1, e^{j2\pi(d/\lambda)\sin\theta_k}, \cdots, e^{j2\pi(d/\lambda)(N-1)\sin\theta_k}\right]^T, \\ \mathbf{a}_t(\theta_k, r_k) &= \left[1, e^{-j4\pi(\Delta f/c)r_k}, \cdots, e^{-j4\pi(\Delta f/c)(M-1)r_k}\right]^T \odot \\ &\quad \cdot \left[1, e^{j2\pi(d/\lambda)\sin(\theta_k)}, \cdots, e^{j2\pi(d/\lambda)(M-1)\sin\theta_k}\right]^T, \end{aligned} \tag{7}$$

where $\mathbf{a}_r(\theta_k) \in \mathbb{C}^{N\times 1}$ and $\mathbf{a}_t(\theta_k, r_k) \in \mathbb{C}^{M\times 1}$.

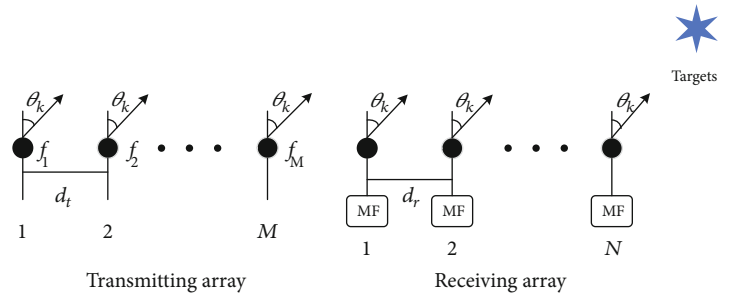

Figure 1: Simplified diagram of a monostatic double-pulse FDA-MIMO radar.

The output of the MF by collecting L snapshots can be described as

$$\mathbf{X} = \mathbf{AS} + \mathbf{N}, \tag{8}$$

where $\mathbf{X} = [\mathbf{x}(1), \mathbf{x}(2), \cdots, \mathbf{x}(L)] \in \mathbb{C}^{MN\times L}$, $\mathbf{S} = [\mathbf{s}(1), \mathbf{s}(2), \cdots, \mathbf{s}(L)] \in \mathbb{C}^{K\times L}$, and $\mathbf{N} = [\mathbf{n}(1), \mathbf{n}(2), \cdots, \mathbf{n}(L)] \in \mathbb{C}^{MN\times L}$.

3. Range and Angle Estimation for Monostatic Double-Pulse FDA-MIMO Radar

In this section, we propose a target localization algorithm with a double-pulse FDA-MIMO radar based on iterative grid refinement to alleviate the problem that grid partition brings about, a heavy computational burden and correlation. Firstly, we decouple the range and angle parameters of the FDA-MIMO radar with two pulses. Then, the improved l_1-SVD method is utilized to estimate the angle and range of the target.

3.1. Angle Estimation for FDA-MIMO Radar. The angle estimates of targets are calculated by transmitting a pulse with a zero frequency increment and avoiding the range parameter. According to (8), the output of the FDA-MIMO radar after MF can be reconstructed by [32]

$$\mathbf{X}_a = \mathbf{A}_a\mathbf{S}_a + \mathbf{N}_a, \tag{9}$$

where $\mathbf{X}_a = [\mathbf{x}_a(1), \mathbf{x}_a(2), \cdots, \mathbf{x}_a(L)] \in \mathbb{C}^{MN\times L}$. $\mathbf{S}_a = [\mathbf{s}_a(1), \mathbf{s}_a(2), \cdots, s_a(L)] \in \mathbb{C}^{K\times L}$ is a transmit signal matrix. $\mathbf{N}_a = [\mathbf{n}_a(1), \mathbf{n}_a(2), \cdots, \mathbf{n}_a(L)] \in \mathbb{C}^{MN\times L}$ stands for the noise matrix. $\mathbf{A}_a = [\mathbf{a}_a(\theta_1), \mathbf{a}_a(\theta_2), \cdots, \mathbf{a}_a(\theta_K)]$ is a $MN \times K$ steering vector matrix, and $\mathbf{a}_a(\theta_k) = \mathbf{a}_{ar}(\theta_k) \otimes \mathbf{a}_{at}(\theta_k)$ with $k = 1, 2, \cdots, K$. Then, the steering vectors of the receiver and transmitter of the k-th target can be defined by

$$\begin{aligned}\mathbf{a}_{at}(\theta_k) &= \left[1, e^{j2\pi(d/\lambda)\ \sin\theta_k}, \cdots, e^{j2\pi(d/\lambda)(M-1)\ \sin\theta_k}\right]^T,\\ \mathbf{a}_{ar}(\theta_k) &= \left[1, e^{j2\pi(d/\lambda)\ \sin\theta_k}, \cdots, e^{j2\pi(d/\lambda)(N-1)\ \sin\theta_k}\right]^T.\end{aligned} \tag{10}$$

We can utilize the sparse recovery method to achieve angle estimates. An overcomplete set of angles $\overline{\theta} = [\overline{\theta}_1, \overline{\theta}_2, \cdots, \overline{\theta}_P]$ is established by sampling the spatial domain range $[-\pi/2, \pi/2]$ uniformly, where $P \gg K$ is the number of grid points. Then, we need to reformulate the signal model (9) into the sparse signal model as

$$\mathbf{X}_a = \bar{\mathbf{A}}_a\bar{\mathbf{S}}_a + \mathbf{N}_a, \tag{11}$$

where $\bar{\mathbf{S}}_a = [\bar{\mathbf{s}}_a(1), \bar{\mathbf{s}}_a(2), \cdots, \bar{\mathbf{s}}_a(L)] \in \mathbb{C}^{P\times L}$ is a sparse matrix. $\bar{\mathbf{A}}_a = [\bar{\mathbf{a}}_a(\overline{\theta}_1), \bar{\mathbf{a}}_a(\overline{\theta}_2), \cdots, \bar{\mathbf{a}}_a(\overline{\theta}_P)] \in \mathbb{C}^{MN\times P}$ is an overcomplete dictionary, and $\bar{\mathbf{a}}_a(\overline{\theta}_p) = \bar{\mathbf{a}}_{ar}(\overline{\theta}_p) \otimes \bar{\mathbf{a}}_{at}(\overline{\theta}_p)$ with $p = 1, 2, \cdots, P$. $\bar{\mathbf{a}}_{at}(\overline{\theta}_p)$ and $\bar{\mathbf{a}}_{ar}(\overline{\theta}_p)$ can be denoted as

$$\begin{aligned}\bar{\mathbf{a}}_{at}\left(\overline{\theta}_p\right) &= \left[1, e^{j2\pi(d/\lambda)\ \sin\overline{\theta}_p}, \cdots, e^{j2\pi(d/\lambda)(M-1)\ \sin\overline{\theta}_p}\right]^T,\\ \bar{\mathbf{a}}_{ar}\left(\overline{\theta}_p\right) &= \left[1, e^{j2\pi(d/\lambda)\ \sin\overline{\theta}_p}, \cdots, e^{j2\pi(d/\lambda)(N-1)\ \sin\overline{\theta}_p}\right]^T.\end{aligned} \tag{12}$$

Then, we utilize the l_1-SVD method to estimate the angle. The SVD result of the matrix $\mathbf{X}_a$ can be represented by [29]

$$\mathbf{X}_a = \mathbf{U}_a\mathbf{Q}_a{\mathbf{V}_a}^T, \tag{13}$$

where $\mathbf{U}_a \in \mathbb{C}^{MN\times MN}$ and $\mathbf{V}_a \in \mathbb{C}^{L\times L}$ are orthogonal matrices and $\mathbf{Q}_a \in \mathbb{C}^{MN\times L}$ is a block matrix. We get a $MN \times K$ matrix $\mathbf{X}_{aSV}$, which contains nearly all the signal power, $\mathbf{X}_{aSV} = \mathbf{U}_a\mathbf{Q}_a\mathbf{D}_K = \mathbf{X}_a\mathbf{V}_a\mathbf{D}_K$. $\mathbf{D}_K = [\mathbf{I}_K, 0] \in \mathbb{C}^{L\times K}$ where $\mathbf{I}_K \in \mathbb{C}^{K\times K}$ is an identity matrix, and $0 \in \mathbb{C}^{(T-K)\times K}$ is a zero matrix. Moreover, suppose $\bar{\mathbf{S}}_{aSV} = \bar{\mathbf{S}}_a\mathbf{V}_a\mathbf{D}_K$ and $\mathbf{N}_{aSV} = \mathbf{N}\mathbf{V}_a\mathbf{D}_K$; we can derive $\mathbf{X}_{aSV}$ as

$$\mathbf{X}_{aSV} = \bar{\mathbf{A}}_a\bar{\mathbf{S}}_{aSV} + \mathbf{N}_{aSV}. \tag{14}$$

$\tilde{s}_{ai}^{(l_2)} = \sqrt{\sum_{k=1}^{K}(s_{ai}^{aSV}(k))^2}$, where $i = 1, 2, \cdots, P$. The sparsity vector $\tilde{\mathbf{s}}_a^{(l_2)}$ corresponds to the space spectrum, which can be calculated by the following constraint optimization problem:

$$\min \left\|\tilde{\mathbf{s}}_a^{(l_2)}\right\|_1, \text{subject to } \left\|\mathbf{X}_{aSV} - \bar{\mathbf{A}}_a\bar{\mathbf{S}}_{aSV}\right\|_2^2 \le \eta_a^2, \tag{15}$$

where η_a denotes the regularization parameter [29] to balance the mismatch degree of the model and the sparsity. According to the chi-squared distribution, the upper bound of $\mathbf{N}_{aSV}$ can be calculated by the regularization parameter η_a [33] with a high probability of 99.9%. Finally, we utilize the second-

order cone (SOC) programming package, such as CVX, to solve the optimization problem in (15). Based on $\tilde{\mathbf{s}}_a^{(l_2)}$, the one-dimensional spectral peak search can be established where the angle estimates correspond to K maximum peaks.

3.2. Range Estimation for FDA-MIMO Radar. The range estimates of targets are calculated by transmitting a pulse with a nonzero frequency increment. The output of the MF by collecting L snapshots can be expressed as (8).

We assume that angle estimates obtained from subsection A are $\bar{\theta} = [\bar{\theta}_1, \bar{\theta}_2, \cdots, \bar{\theta}_K]^T$. To get the range estimates, we utilize the sparse recovery method. An overcomplete set of ranges $\bar{\mathbf{r}} = [\bar{r}_1, \bar{r}_2, \cdots, \bar{r}_W]$ is established by sampling the spatial domain range $[0, c/2\Delta f]$ uniformly, where W is the number of grid points and $c/2\Delta f$ denotes the maximum unambiguous range [34]. We stack the range complete set corresponding to K angles into a large row vector $\tilde{\mathbf{r}} = [\tilde{r}_{(\bar{\theta}_1,1)}, \tilde{r}_{(\bar{\theta}_1,2)}, \cdots, \tilde{r}_{(\bar{\theta}_1,W)}, \tilde{r}_{(\bar{\theta}_2,1)}, \cdots, \tilde{r}_{(\bar{\theta}_K,W-1)}, \tilde{r}_{(\bar{\theta}_K,W)}]$ to obtain automatically paired range and angle estimates. Then, we need to construct the signal model of (8) into a sparse signal model as

$$\mathbf{X} = \bar{\mathbf{A}}_r \bar{\mathbf{S}}_r + \mathbf{N}, \tag{16}$$

where $\bar{\mathbf{S}}_r = [\bar{\mathbf{s}}_r(1), \bar{\mathbf{s}}_r(2), \cdots, \bar{\mathbf{s}}_r(L)] \in \mathbb{C}^{KW \times L}$ denotes a sparse matrix. $\bar{\mathbf{A}}_r = [\bar{\mathbf{a}}_r(\bar{\theta}_1, \bar{r}_1), \bar{\mathbf{a}}_r(\bar{\theta}_1, \bar{r}_2), \cdots, \bar{\mathbf{a}}_r(\bar{\theta}_K, \bar{r}_{W-1}), \bar{\mathbf{a}}_r(\bar{\theta}_K, \bar{r}_W)] \in \mathbb{C}^{MN \times KW}$ is a known overcomplete dictionary, and $\bar{\mathbf{a}}_r(\bar{\theta}_k, \bar{r}_w) = \bar{\mathbf{a}}_{rr}(\bar{\theta}_k) \otimes \bar{\mathbf{a}}_{rt}(\bar{\theta}_k, \bar{r}_w)$ with $k = 1, 2, \cdots, K$ and $w = 1, 2, \cdots, W$. $\bar{a}_{rt}(\bar{\theta}_k, \bar{r}_w)$ and $\bar{a}_{rr}(\bar{\theta}_k)$ can be defined as

$$\begin{aligned} \bar{\mathbf{a}}_{rt}\left(\bar{\theta}_k, \bar{r}_w\right) &= \left[1, e^{-j4\pi(\Delta f/c)\bar{r}_w}, \cdots, e^{-j4\pi(M-1)(\Delta f/c)\bar{r}_w}\right]^T \mathrm{e} \\ &\quad \cdot \left[1, e^{j2\pi(d/\lambda)\ \sin\left(\bar{\theta}_k\right)}, \cdots, e^{j2\pi(d/\lambda)\ \sin\left(\bar{\theta}_k\right)}\right]^T, \\ \bar{\mathbf{a}}_{rr}\left(\bar{\theta}_k\right) &= \left[1, e^{j2\pi(d/\lambda)\ \sin\left(\bar{\theta}_k\right)}, \cdots, e^{j2\pi(d/\lambda)(N-1)\ \sin\left(\bar{\theta}_k\right)}\right]^T. \end{aligned} \tag{17}$$

Then, we utilize the l_1-SVD method to estimate the range. The SVD result of the matrix $\mathbf{X}$ can be expressed as [29]

$$\mathbf{X} = \mathbf{U}_r \mathbf{Q}_r \mathbf{V}_r^T, \tag{18}$$

where $\mathbf{U}_r \in \mathbb{C}^{MN \times MN}$ and $\mathbf{V}_r \in \mathbb{C}^{L \times L}$ are orthogonal matrices and $\mathbf{Q}_r \in \mathbb{C}^{MN \times L}$ is a block matrix. We can get a $MN \times K$ matrix $\mathbf{X}_{rSV}$, which contains nearly all the signal power, $\mathbf{X}_{rSV} = \mathbf{U}_r \mathbf{Q}_r \mathbf{D}_K = \mathbf{X}_r \mathbf{V}_r \mathbf{D}_K$. Besides, suppose $\bar{\mathbf{S}}_{rSV} = \bar{\mathbf{S}}_r \mathbf{V}_r \mathbf{D}_K$ and $\mathbf{N}_{rSV} = \mathbf{N}\mathbf{V}_r \mathbf{D}_K$; we can derive the expression for $\mathbf{X}_{rSV}$ as

$$\mathbf{X}_{rSV} = \bar{\mathbf{A}}_r \bar{\mathbf{S}}_{rSV} + \mathbf{N}_{rSV}. \tag{19}$$

$\tilde{s}_{ri}^{(l_2)} = \sqrt{\sum_{k=1}^{K} \left(s_{ri}^{rSV}(k)\right)^2}$, where $i = 1, 2, \cdots, KW$. The sparsity of $\tilde{\mathbf{s}}_r^{(l_2)}$ corresponds to the sparsity of the space spectrum, which can be calculated by the following constraint optimization problem:

$$\min \left\| \tilde{\mathbf{s}}_r^{(l_2)} \right\|_1, \text{ subject to } \left\| \mathbf{X}_{rSV} - \bar{\mathbf{A}}_r \bar{\mathbf{S}}_{rSV} \right\|_2^2 \le \eta_r^2. \tag{20}$$

According to the chi-squared distribution, the upper bound of the $\mathbf{N}_{rSV}$ power can be calculated as the regularization parameter η_r [33] with a high probability of 99.9%. Finally, we utilize the SOC programming package, such as CVX, to solve the optimization problem in (20). Based on $\tilde{\mathbf{s}}_r^{(l_2)}$, the one-dimensional spectral peak search can be established where the range estimates correspond to K maximum peaks.

3.3. Grid Refinement. Since it is impossible that all parameter estimates fall on the grid points, the refining operation for the grid is required, which will bring high computational complexity and produce highly correlated atoms. To tackle the problems, we propose an improved iterative grid refinement algorithm. For example, the algorithm steps of range estimation are given as follows:

(1) Set refinement times $o = 1$. A simple grid $\mathbf{r}^{(o)}$ is constructed by discretizing the interval between 0 and $c/2\Delta f$ to estimate the target parameters. The grid spacing is B_o

(2) Use the proposed method in subsection B to get $\tilde{\mathbf{r}}_o = [r_1, r_2, \cdots, r_K]$ and $F_o^r = \left| \|\mathbf{R}\|_2 - \|\mathbf{R}_o^r\|_2 \right|$. Then, set $o = o + 1$

(3) According to the range estimates in step 2, a new grid $\mathbf{r}^{(o)}$ composed of K subgrids is constructed, where K subgrids are $\tilde{r}_1, \tilde{r}_2, \cdots, \tilde{r}_K$ and $\tilde{r}_i$ is a grid established by sampling the spatial domain range with $[r_i - B_o, r_i + B_o]$ uniformly, and $i = 1, 2, \cdots, K$. Set grid spacing $B_o = B_{o-1}/100$

(4) Return to step 2 until $F_{o-1}^r < F_o^r$, the final range estimates can be obtained as $\tilde{\mathbf{r}}_{o-1}$

In the proposed algorithm, we use F to improve the error between real parameters and their estimates to get a trade-off between the high-precision grid and the atomic correlation. The detailed steps of the proposed sparse recovery algorithm based on a double-pulse FDA-MIMO radar are summarized in Algorithm 1.

Remark 2. The main computational complexity of the proposed algorithm is the singular value decomposition and the SOC programming problem. The singular value decomposition of $\mathbf{X}$ and $\mathbf{X}_a$ requires altogether $O\{2U(MN)^2 + 2MNUL^2\}$ flops, and it takes $O\{(K^2W)^3 + (PK)^3 + 2(U-1)(K^2G)^3\}$ flops to solve the above SOC programming problem, where U denotes the number of iterations and G represents the number of refinement grid points for each target. Compared with the U-ESPRIT algorithm [20], the proposed algorithm requires more computation. However, this algorithm has outstanding advantages, which can not only adapt

(1) The FDA-MIMO radar transmits a pulse with a zero frequency increment to obtain the received signal $\mathbf{X}_a$
(2) The sparse vector $\tilde{\mathbf{s}}_a^{(l_2)}$ is obtained by CVX optimization of (15). Angle estimates are realized by searching K maximum values through a one-dimensional spectrum of $\tilde{\mathbf{s}}_a^{(l_2)}$
(3) Use the method in subsection C to optimize the angle estimates in step 2. Then, the refined angle estimates can be received as $[\theta_1, \theta_2, \cdots, \theta_K]$
(4) The FDA-MIMO radar transmits a pulse with a nonzero frequency increment to obtain the received signal $\boldsymbol{X}$
(5) The sparse vector $\tilde{\mathbf{s}}_r^{(l_2)}$ is obtained by CVX optimization of (20). Range estimates are realized by searching K maximum values through a one-dimensional spectrum of $\tilde{\mathbf{s}}_r^{(l_2)}$
(6) Use the method in subsection C to optimize the range estimates in step 5. Then, the range estimates can be obtained as $[r_1, r_2, \cdots, r_K]$, and get automatically paired range and angle estimates (θ_k, r_k), for $k = 1, 2, \cdots, K$

Algorithm 1: An accurate sparse recovery algorithm for double-pulse FDA-MIMO radar.

to the scene of insufficient snapshots and high target correlation but also provide higher precision and resolution.

Remark 3. We assume that angle estimates obtained from subsection A are $\overline{\theta}_1, \overline{\theta}_2, \cdots, \overline{\theta}_K$, respectively. Therefore, we can construct a simplified overcomplete dictionary containing range and angle information via adding a sparse grid of the range dimension. By solving the SOC programming problem in (20), a $KW \times 1$ sparse vector $\tilde{\mathbf{s}}_r^{(l_2)}$ can be obtained, where the first W elements represent the range estimates of the target with angle $\overline{\theta}_1$, the $W+1$ to $2W$ represent the range estimates of the target with angle $\overline{\theta}_2$, and the last W elements represent the range estimates of the target with angle $\overline{\theta}_K$. Hence, the corresponding angle can be found through the position of the element in the sparse space spectrum $\tilde{\mathbf{s}}_r^{(l_2)}$ to obtain automatically paired range and angle estimates.

Remark 4. In this paper, we utilize F to improve the error between real parameters and their estimates. F can be written as F^a in the angle estimates, which is defined by $|\|\mathbf{R}_a\|_2 - \|\mathbf{R}^a\|_2|$, where $\mathbf{R}_a = \mathbf{X}_a\mathbf{X}_a^H$ and $\mathbf{R}^a = (\mathbf{A}^a\mathbf{S}_a)(\mathbf{A}^a\mathbf{S}_a)^H$. $\mathbf{A}^a = [\mathbf{a}_a(\overline{\theta}_1), \mathbf{a}_a(\overline{\theta}_2), \cdots, \mathbf{a}_a(\overline{\theta}_K)]$ is a new steering vector matrix constructed by θ. $\theta = [\overline{\theta}_1, \overline{\theta}_2, \cdots, \overline{\theta}_K]^T$ is the angle estimate for each iteration. F can be written as F^r in the range estimates, which is defined by $|\|\mathbf{R}\|_2 - \|\mathbf{R}^r\|_2|$, where $\mathbf{R} = \mathbf{X}\mathbf{X}^H$ and $\mathbf{R}^r = (\mathbf{A}^r\mathbf{S})(\mathbf{A}^r\mathbf{S})^H$. $\mathbf{A}^r = [\bar{\mathbf{a}}(\widehat{\theta}_1, \widehat{r}_1), \bar{\mathbf{a}}(\widehat{\theta}_2, \widehat{r}_2), \cdots, \bar{\mathbf{a}}(\widehat{\theta}_K, \widehat{r}_K)]$ is a new steering vector matrix constructed by $\widehat{\theta}$ and $\widehat{\mathbf{r}}$. $\widehat{\theta} = [\theta\wedge_1, \theta\wedge_2, \cdots, \theta\wedge_K]^T$ is the angle estimate in advance, and $\widehat{\mathbf{r}} = [r\wedge_1, r\wedge_2, \cdots, r\wedge_K]^T$ denotes the range estimate for each iteration.

4. CRLB Analysis

In this section, we derive the CRLB results with regard to the angle and range. According to (8) and (9), we can rewrite the signal model as vector

$$\mathbf{x}_{\text{new}} = \mathbf{a}_{\text{new}}(\theta_k, r_k) \cdot s + \mathbf{v}, \tag{21}$$

where the $\mathbf{v}$ is the normalized Gaussian noise with zero mean and unit variance $\mathbf{I}$. $\mathbf{a}_{\text{new}}(\theta_k, r_k) \in \mathbb{C}^{2MN\times 1}$ is the equivalent steering vector and can be presented by

$$\mathbf{a}_{\text{new}}(\theta_k, r_k) = \left[\mathbf{a}(\theta_k, r_k)|_{\Delta f=0}, \mathbf{a}(\theta_k, r_k)\right]^T, \tag{22}$$

where

$$\begin{aligned} \mathbf{a}(\theta_k, r_k)\big|_{\Delta f=0} &= \mathbf{a}_{ar}(\theta_k) \otimes \mathbf{a}_{at}(\theta_k), \\ \mathbf{a}(\theta_k, r_k) &= \mathbf{a}_r(\theta_k) \otimes \mathbf{a}_t(\theta_k, r_k). \end{aligned} \tag{23}$$

Assuming that there are K targets, the Fisher information matrix (FIM) is [35]

$$\mathbf{J} = \begin{bmatrix} J_{\theta_k\theta_k} & J_{\theta_k r_k} \\ J_{r_k\theta_k} & J_{r_k r_k} \end{bmatrix}, \tag{24}$$

where $k = 1, 2, \cdots, K$.

$$\begin{aligned} J_{\theta_k\theta_k} &= \frac{2L}{\sigma^2}\ \text{Re}\left[\left(\frac{d\varepsilon}{d\theta_k}\right)^H \Gamma^{-1}\left(\frac{d\varepsilon}{d\theta_k}\right)\right], \\ J_{\theta_k r_k} &= \frac{2L}{\sigma^2}\ \text{Re}\left[\left(\frac{d\varepsilon}{d\theta_k}\right)^H \Gamma^{-1}\left(\frac{d\varepsilon}{dr_k}\right)\right], \\ J_{r_k\theta_k} &= \frac{2L}{\sigma^2}\ \text{Re}\left[\left(\frac{d\varepsilon}{dr_k}\right)^H \Gamma^{-1}\left(\frac{d\varepsilon}{d\theta_k}\right)\right], \\ J_{r_k r_k} &= \frac{2L}{\sigma^2}\ \text{Re}\left[\left(\frac{d\varepsilon}{dr_k}\right)^H \Gamma^{-1}\left(\frac{d\varepsilon}{dr_k}\right)\right], \end{aligned} \tag{25}$$

where σ^2 represents the noise power, $\varepsilon = a_{\text{new}}(\theta_k, r_k)$, and

$\Gamma = \mathbf{I}$. $d\varepsilon/d\theta_k$ and $d\varepsilon/dr_k$ can be expressed as

$$\frac{d\varepsilon}{d\theta_k} = \left[\frac{\partial a_{ar}(\theta_k)}{\partial \theta_k} \otimes a_{ar}(\theta_k) + a_{ar}(\theta_k) \otimes \frac{\partial a_{at}(\theta_k)}{\partial \theta_k}, \frac{\partial a_r(\theta_k)}{\partial \theta_k} \otimes a_t(\theta_k, r_k) + a_r(\theta_k) \otimes \frac{\partial a_t(\theta_k, r_k)}{\partial \theta_k}\right],$$

$$\frac{d\varepsilon}{dr_k} = \left[0, a_r(\theta_k) \otimes \frac{\partial a_t(\theta_k, r_k)}{\partial r_k}\right],$$

$$\frac{\partial a_{ar}(\theta_k)}{a\theta_k} = j2\pi \frac{d}{\lambda} \cos(\theta_k) \begin{bmatrix} 0 & & \\ & \ddots & \\ & & N-1 \end{bmatrix} a_{ar}(\theta_k),$$

$$\frac{\partial a_{at}(\theta_k)}{a\theta_k} = j2\pi \frac{d}{\lambda} \cos(\theta_k) \begin{bmatrix} 0 & & \\ & \ddots & \\ & & M-1 \end{bmatrix} a_{at}(\theta_k),$$

$$\frac{\partial a_r(\theta_k)}{a\theta_k} = j2\pi \frac{d}{\lambda} \cos(\theta_k) \begin{bmatrix} 0 & & \\ & \ddots & \\ & & N-1 \end{bmatrix} a_r(\theta_k),$$

$$\frac{\partial a_t(\theta_k, r_k)}{a\theta_k} = j2\pi \frac{d\cos(\theta_k)}{\lambda} \begin{bmatrix} 0 & & \\ & \ddots & \\ & & M-1 \end{bmatrix} a_t(\theta_k, r_k),$$

$$\frac{\partial a_t(\theta_k, r_k)}{ar_k} = -j4\pi \frac{\Delta f}{c} \begin{bmatrix} 0 & & \\ & \ddots & \\ & & M-1 \end{bmatrix} a_t(\theta_k, r_k). \quad (26)$$

The CRLB for the range and angle can be expressed as

$$\begin{aligned} \mathrm{CRLB}_{\theta_k} &= \left[\mathbf{J}^{-1}\right]_{1,1}, \\ \mathrm{CRLB}_{r_k} &= \left[\mathbf{J}^{-1}\right]_{2,2}. \end{aligned} \quad (27)$$

5. Numerical Simulation Results

In this section, we demonstrate the superiority of the proposed algorithm via simulation, where $M = N = 8$ and $d = \lambda/2$. The carrier frequency f_0 is 10 GHz, the frequency increment Δf is 0 kHz in angle estimation, and the frequency increment Δf is 1 kHz in range estimation.

5.1. Simple Process of Target Estimation. Suppose $K = 3$ narrowband targets with angles $\theta_1 = -20^\circ$ and $\theta_2 = \theta_3 = 40^\circ$ and ranges $r_1 = 21000$m, $r_2 = 34000$m, and $r_3 = 54000$m, respectively. We set SNR = 10 dB, and the number of snapshots is

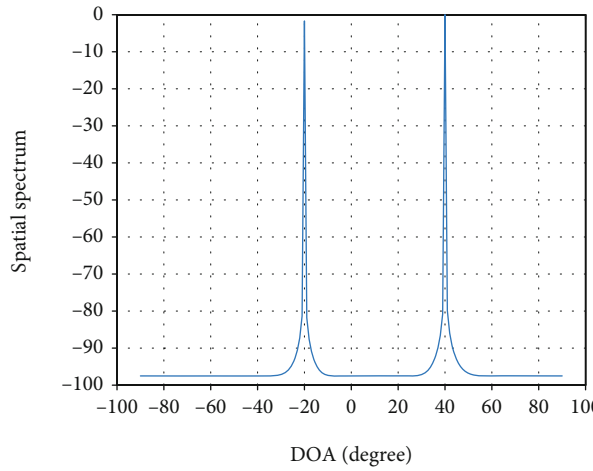

Figure 2: The spatial spectrum of angle estimation.

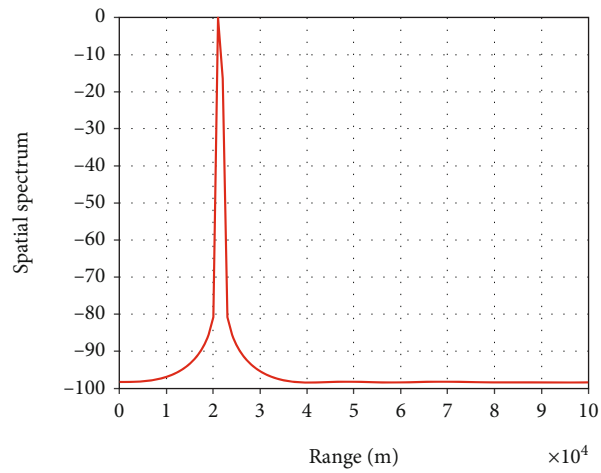

Figure 3: Range estimation of the target with angle θ_1.

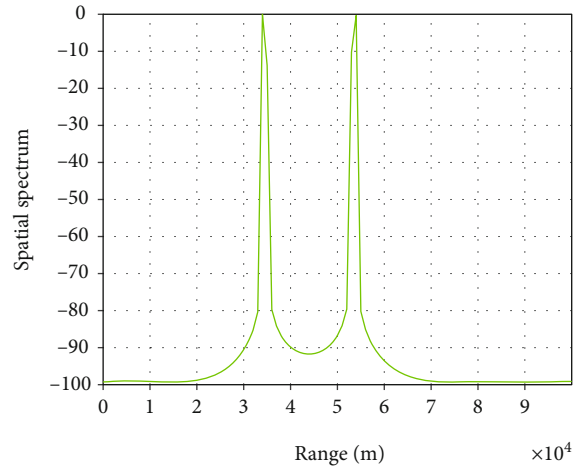

Figure 4: Range estimation of the target with angle θ_2.

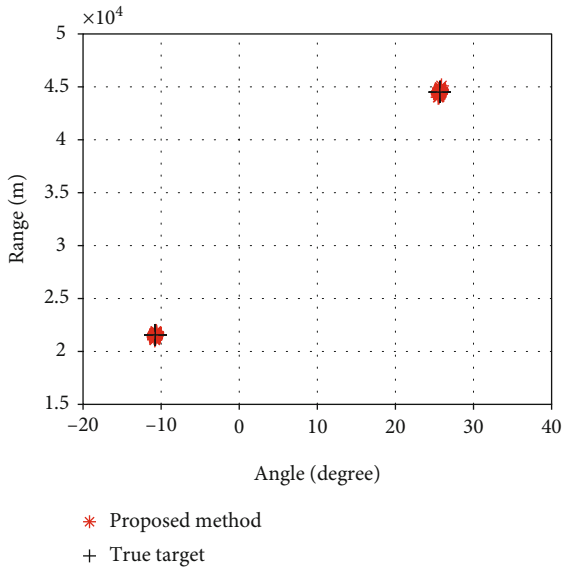

Figure 5: Range and angle estimation results using the proposed algorithm.

50. Figure 2 depicts the spatial spectrum of the sparse vector $\tilde{\mathbf{s}}_a^{(l_2)}$ for angle estimates in the proposed algorithm. Since there are two targets from the same direction, it is necessary to extract the range estimates of targets. Figures 3 and 4 give the spatial spectrums of the first W elements and the last W elements of $\tilde{\mathbf{s}}_r^{(l_2)}$, respectively, where the first W elements of $\tilde{\mathbf{s}}_r^{(l_2)}$ represent range estimates of the target with angle θ_1, and the last W elements of $\tilde{\mathbf{s}}_r^{(l_2)}$ represent range estimates of the target with angles θ_2 and θ_3. Figure 3 shows the range estimates of the target with angle θ_1, and Figure 4 shows the range estimates of the target with angles θ_2 and θ_3.

5.2. Detection and Estimation Performance. In this subsection, we carry out a series of simulations under different conditions to verify the superiority of the proposed algorithm. The ESPRIT method [19] and the U-ESPRIT method [20] are compared with the proposed algorithm. We assume that the frequency increment and the carrier frequency of the above algorithms are 1 kHz and 10 GHz, respectively. Suppose that two targets are located: $(-10.75^\circ, 21565\,\text{m})$ and $(25.68^\circ, 44505\,\text{m})$. The grids of the angle and range for the proposed algorithm are $[-90^\circ : 1^\circ : 90^\circ]$ and $[0 : 1 : 150]$ km, respectively. The root mean square errors (RMSEs) for the range and angle are defined as

$$\begin{aligned} \text{RMSE}_\theta &= \sqrt{\frac{1}{\rho K}\sum_{i=1}^{\rho}\sum_{k=1}^{K}(\theta_{ik}-\theta_k)^2}, \\ \text{RMSE}_r &= \sqrt{\frac{1}{\rho K}\sum_{i=1}^{\rho}\sum_{k=1}^{K}(r_{ik}-r_k)^2}, \end{aligned} \tag{28}$$

where $\rho = 100$ is the number of Monte Carlo experiments. θ_{ik} and r_{ik} represent the estimates of θ_k and r_k in the i-th Monte Carlo experiment.

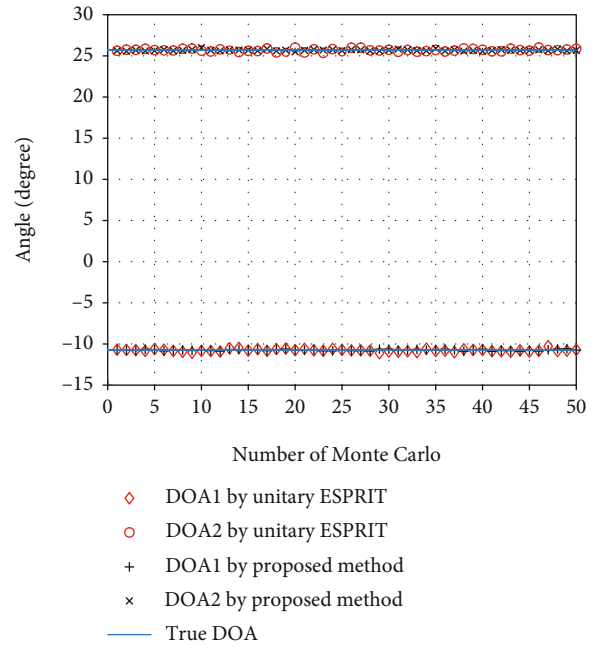

Figure 6: Comparison of DOA estimated results of 50 independent simulations.

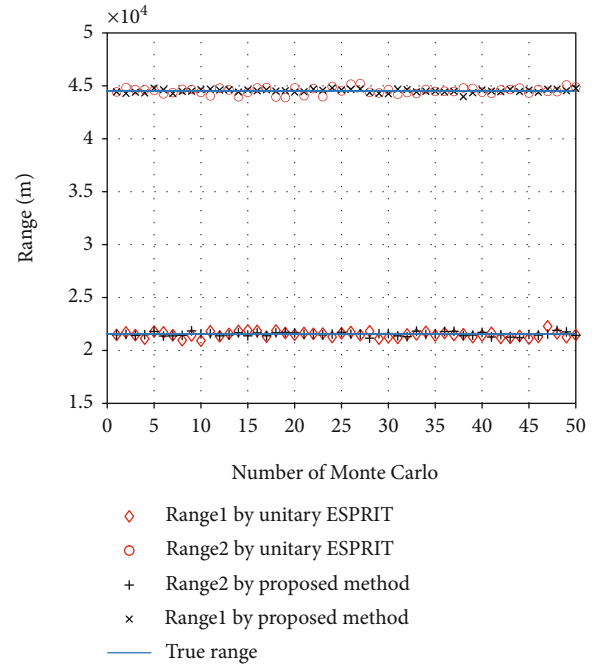

Figure 7: Comparison of range estimated results of 50 independent simulations.

The angle-range estimation results are exhibited in Figure 5 for FDA-MIMO radar using the proposed algorithm in which Monte Carlo trials are implemented 100 times. Moreover, the results of U-ESPRIT and the proposed algorithm are provided for comparison with the proposed

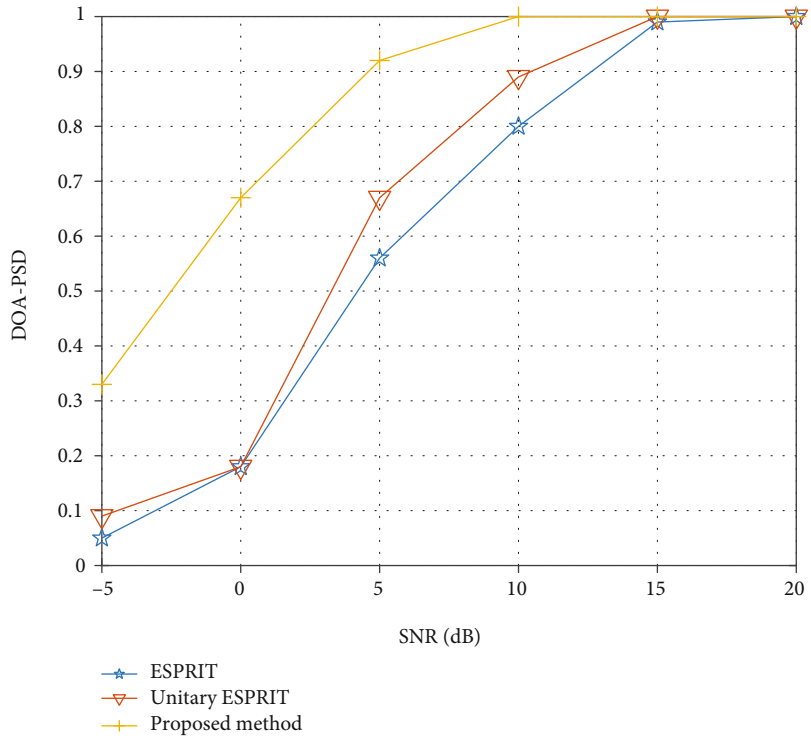

Figure 8: PSD versus SNR for angle estimation.

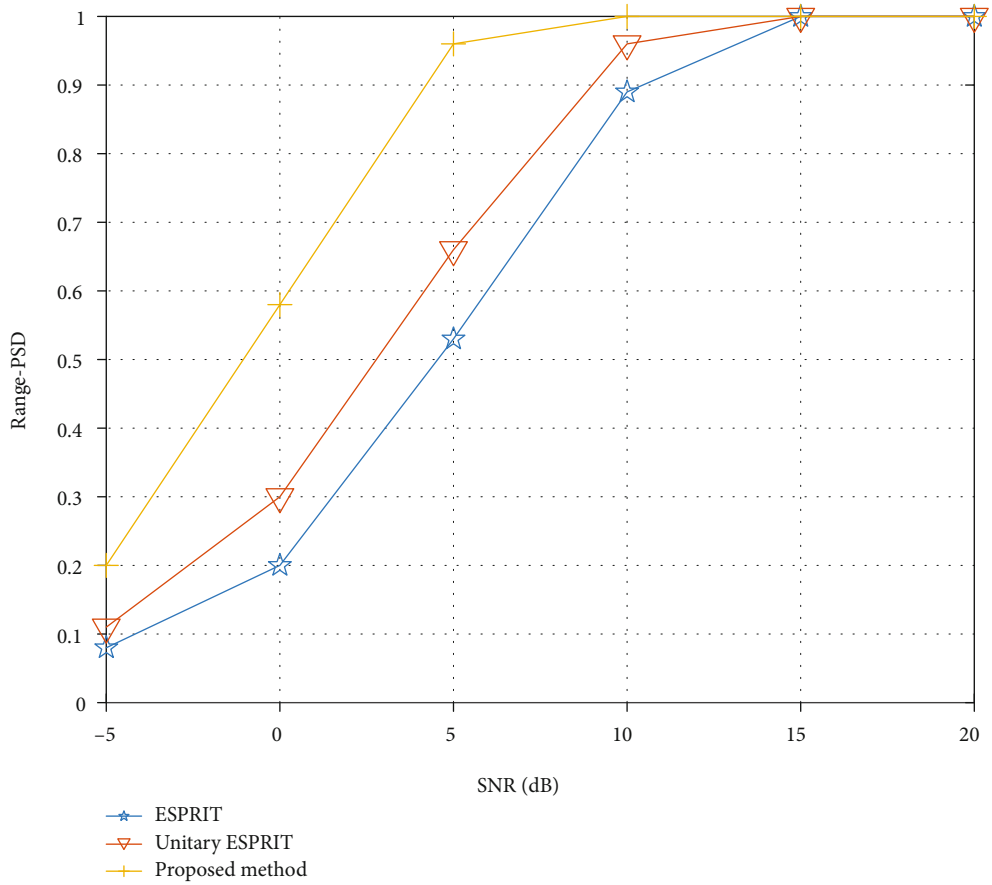

Figure 9: PSD versus SNR for range estimation.

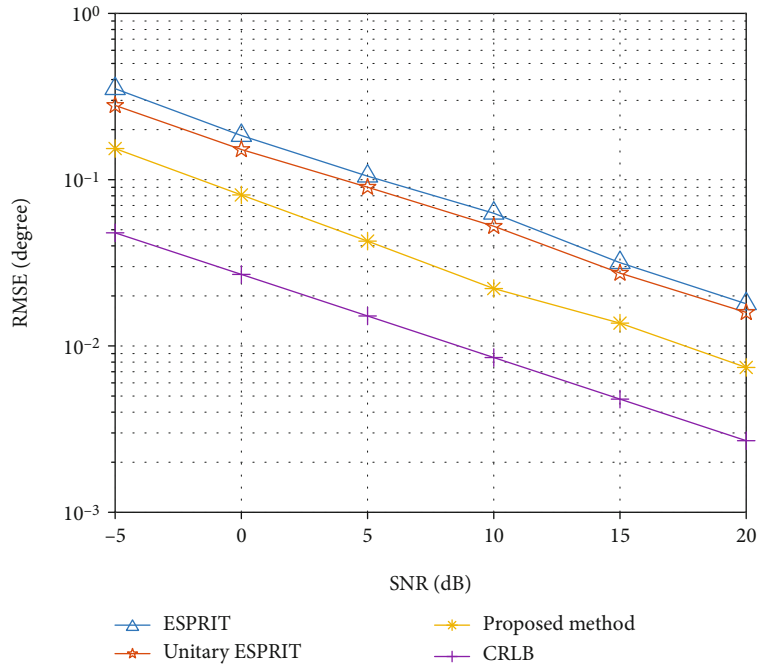

Figure 10: RMSE results of angle estimation versus SNR.

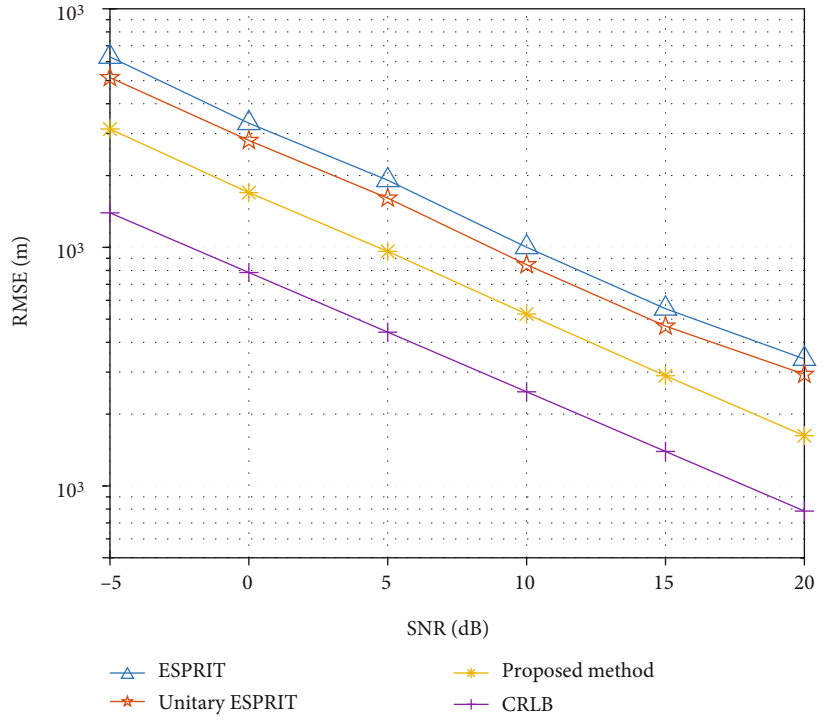

Figure 11: RMSE results of range estimation versus SNR.

algorithm in Figures 6 and 7, where SNR = 0 dB and $L = 50$. According to the results in Figure 5, we can conclude that the proposed algorithm can achieve precise matching of the range and angle. The angles and ranges of the two targets can be accurately estimated with a small number of snapshots. As can be seen from Figures 6 and 7, the parameter estimates of the proposed algorithm can considerably approach the real ones.

Figures 8 and 9 give the probability of successful detection (PSD) versus SNR for angle and range estimation in different algorithms, respectively, where $L = 50$. With regard to angle estimation, we define the successful detection if the

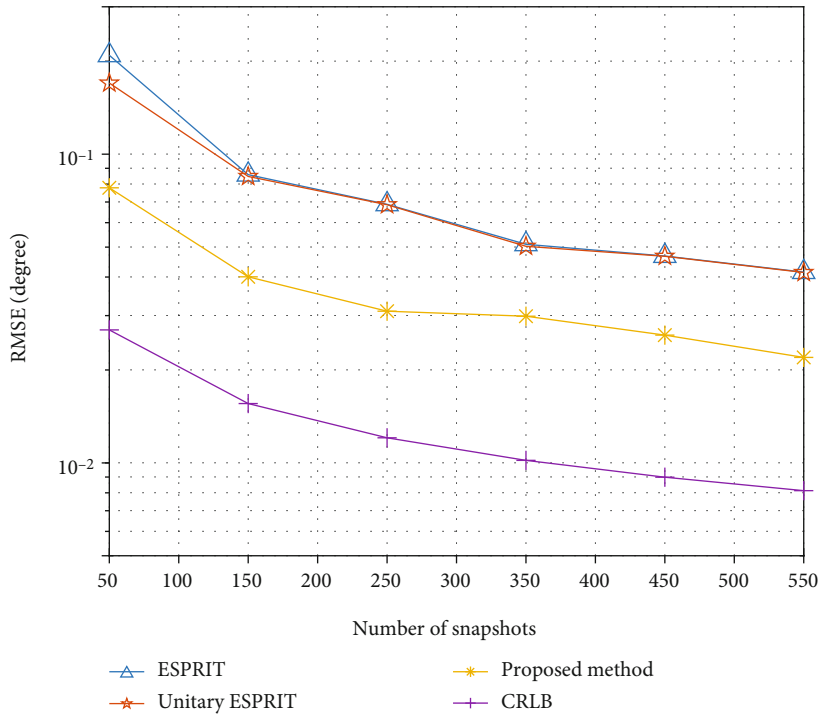

Figure 12: RMSE results of angle estimation versus snapshots.

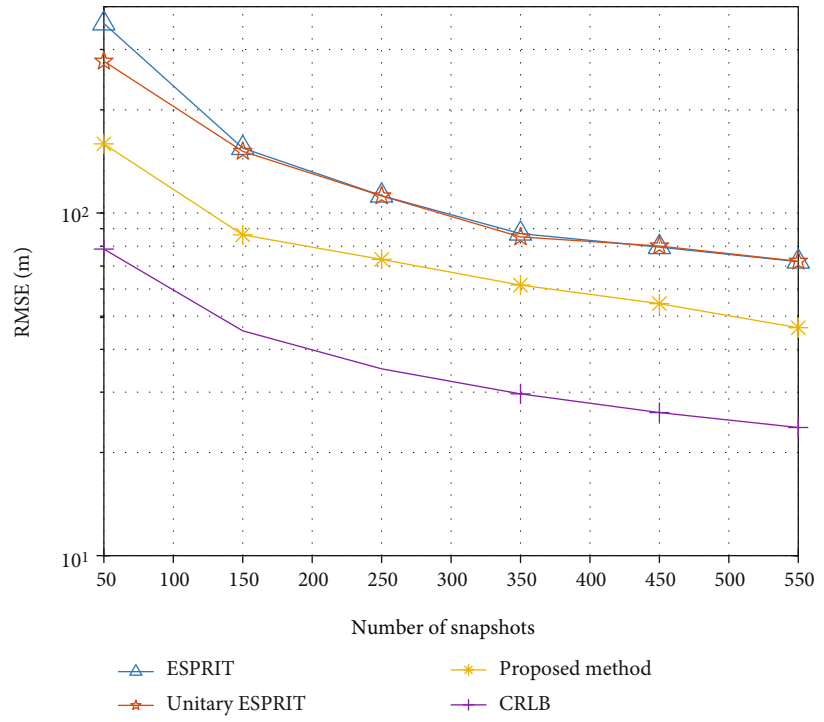

Figure 13: RMSE results of range estimation versus snapshots.

estimation result θ_{ik} satisfies $|\theta_{ik} - \theta_k| \leq 0.1^\circ$. The detection is successful if the estimation result r_{ik} satisfies $|r_{ik} - r_k| \leq 200$ m with regard to range estimation. As can be seen from Figures 8 and 9, the PSD of the proposed algorithm is superior to those of other algorithms under the same condition. Besides, with the increase of SNR, the proposed algorithm can achieve the PSD of 100% when SNR = 10 dB.

Figures 10 and 11 give the RMSE results of the angle and range estimates versus SNR with $L = 50$, respectively. It is obvious that the RMSE results gradually decrease with the

increase of SNR, and in particular, the algorithm outperforms the other methods in range and angle estimation.

Figures 12 and 13 depict the RMSE results of the angle and range estimates versus snapshots, respectively, where SNR = 0 dB. As can be seen from Figures 12 and 13, the RMSE results of all algorithms improve with the increase of snapshots. Besides, the proposed method can obtain more accurate range and angle estimates than the other methods with the same number of snapshots.

6. Conclusion

In this paper, an accurate sparse recovery algorithm based on a double-pulse FDA-MIMO radar is proposed. In the proposed algorithm, we decouple the range and angle parameters of the FDA-MIMO radar with two pulses. Grid partition will bring high computational complexity. Therefore, we adopt an iterative grid refinement method to alleviate the above limitation on parameter estimation and propose a new iteration criterion to improve the error between real parameters and their estimates to get a trade-off between the high-precision grid and the atomic correlation. Compared with the subspace-based algorithms, the proposed algorithm performs better in simulation. Massive simulation results have certified that the proposed algorithm is prominent for parameter estimation of FDA-MIMO radar.

Data Availability

No data were used to support this study.

Conflicts of Interest

The authors declare that there is no conflict of interest regarding the publication of this paper.

Acknowledgments

This work is supported by the Key Research and Development Project of Hainan Province (No. ZDYF2019011), the National Natural Science Foundation of China (Nos. 61701144, 61861015, and 61961013), the Program of Hainan Association for Science and Technology Plans to Youth R&D Innovation (No. QCXM201706), the scientific research projects of University in Hainan Province (No. Hnky2018ZD-4), the Young Elite Scientists Sponsorship Program by CAST (No. 2018QNRC001), and the Scientific Research Setup Fund of Hainan University (No. KYQD (ZR) 1731).

References

[1] C. Gentile, N. Alsindi, R. Raulefs, and C. Teolis, *Geoloc Techniques: Principles and Applications*, Springer, 2012.

[2] D. Ribas, P. Ridao, and J. Neira, *Underwater Slam for Structured Environments Using an Imaging Sonar*, Springer, 2010.

[3] M. Skolnik, *Radar Handbook Third Edition*, McGraw-Hill, 2008.

[4] H. Krim and M. Viberg, "Two decades of array signal processing research: the parametric approach," *IEEE Signal Processing Magazine*, vol. 13, no. 4, pp. 67–94, 1996.

[5] E. Fishler, A. Haimovich, R. Blum, D. Chizhik, L. Cimini, and R. Valenzuela, "MIMO radar: an idea whose time has come," in *Proceedings of the 2004 IEEE Radar Conference (IEEE Cat. No.04CH37509)*, pp. 71–78, Philadelphia, PA, USA, 2004.

[6] D. W. Bliss and K. W. Forsythe, "Multiple-input multiple-output (MIMO) radar and imaging: degrees of freedom and resolution," in *The Thrity-Seventh Asilomar Conference on Signals, Systems & Computers, 2003*, pp. 54–59, Pacific Grove, CA, USA, 2003.

[7] L. Wan, X. Kong, and F. Xia, "Joint range-Doppler-angle estimation for intelligent tracking of moving aerial targets," *IEEE Internet of Things Journal*, vol. 5, no. 3, pp. 1625–1636, 2018.

[8] H. Huang, Y. Song, J. Yang, G. Gui, and F. Adachi, "Deep-learningbased millimeter-wave massive MIMO for hybrid precoding," *IEEE Transactions on Vehicular Technology*, vol. 63, no. 3, pp. 3027–3032, 2019.

[9] H. Huang, J. Yang, H. Huang, Y. Song, and G. Gui, "Deep learning for super-resolution channel estimation and DOA estimation based massive MIMO system," *IEEE Transactions on Vehicular Technology*, vol. 67, no. 9, pp. 8549–8560, 2018.

[10] X. Wang, L. Wan, M. Huang, C. Shen, and K. Zhang, "Polarization channel estimation for circular and non-circular signals in massive MIMO systems," *IEEE Journal of Selected Topics in Signal Processing*, vol. 13, no. 5, pp. 1001–1016, 2019.

[11] J. J. Zhang and A. Papandreou-Suppappola, "MIMO radar with frequency diversity," in *2009 International Waveform Diversity and Design Conference*, pp. 208–212, Kissimmee, FL, USA, 2009.

[12] P. F. Sammartino, C. J. Baker, and H. D. Griffiths, "Frequency diverse MIMO techniques for radar," *IEEE Transactions on Aerospace and Electronic Systems*, vol. 49, no. 1, pp. 201–222, 2013.

[13] J. Xu, G. Liao, S. Zhu, L. Huang, and H. C. So, "Joint range and angle estimation using MIMO radar with frequency diverse array," *IEEE Transactions on Signal Processing*, vol. 63, no. 13, pp. 3396–3410, 2015.

[14] P. F. Sammartino, C. J. Baker, and H. D. Griffiths, "Range-angle dependent waveform," in *2010 IEEE Radar Conference*, pp. 511–515, Washington, DC, USA, 2010.

[15] P. Antonik, M. C. Wicks, H. D. Griffiths, and C. J. Baker, "Frequency diverse array radars," in *2006 IEEE Conference on Radar*, pp. 215–217, Verona, NY, USA, 2006.

[16] W. Wang, "Frequency diverse array antenna: new opportunities," *IEEE Antennas and Propagation Magazine*, vol. 57, no. 2, pp. 145–152, 2015.

[17] W. Wang, "Overview of frequency diverse array in radar and navigation applications," *IET Radar Sonar Navigation*, vol. 10, no. 6, pp. 1001–1012, 2016.

[18] W. Wang, "Range-angle dependent transmit beampattern synthesis for linear frequency diverse arrays," *IEEE Transactions on Antennas and Propagation*, vol. 61, no. 8, pp. 4073–4081, 2013.

[19] B. Li, W. Bai, and G. Zheng, "Successive ESPRIT algorithm for joint DOA-range-polarization estimation with polarization sensitive FDA-MIMO radar," *IEEE Access*, vol. 6, pp. 36376–36382, 2018.

[20] F. Liu, X. Wang, M. Huang, and L. Wan, "A novel unitary ESPRIT algorithm for monostatic FDA-MIMO radar," *Sensors*, vol. 20, p. 827, 2020.

[21] J. Xiong, W. Wang, and K. Gao, "FDA-MIMO radar range–angle estimation: CRLB, MSE, and resolution analysis," *IEEE Transactions on Aerospace and Electronic Systems*, vol. 54, no. 1, pp. 284–294, 2018.

[22] X. Wang, L. Wang, X. Li, and G. Bi, "Nuclear norm minimization framework for DOA estimation in MIMO radar," *Signal Processing*, vol. 135, pp. 147–152, 2017.

[23] C. Zhou, Y. Gu, X. Fan, Z. Shi, G. Mao, and Y. D. Zhang, "Direction-of-arrival estimation for coprime array via virtual array interpolation," *IEEE Transactions on Signal Processing*, vol. 66, no. 22, pp. 5956–5971, 2018.

[24] Z. Shi, C. Zhou, Y. Gu, N. A. Goodman, and F. Qu, "Source estimation using coprime array: a sparse reconstruction perspective," *IEEE Sensors Journal*, vol. 17, no. 3, pp. 755–765, 2017.

[25] X. Wang, W. Wang, J. Liu, and X. Li, "A sparse representation scheme for angle estimation in monostatic MIMO radar," *Signal Processing*, vol. 104, pp. 258–263, 2014.

[26] L. Wan, G. Han, L. Shu, and N. Feng, "The critical patients localization algorithm using sparse representation for mixed signals in emergency healthcare system," *IEEE Systems Journal*, vol. 12, no. 1, pp. 52–63, 2018.

[27] M. Tipping, "Sparse Bayesian learning and the relevance vector machine," *Mach Learn Res*, vol. 1, pp. 211–244, 2001.

[28] L. Zhao, G. Bi, L. Wang, and H. Zhang, "An improved autocalibration algorithm based on sparse Bayesian learning framework," *IEEE Signal Processing Letters*, vol. 20, no. 9, 2013.

[29] D. Malioutov, M. Cetin, and A. S. Willsky, "A sparse signal reconstruction perspective for source localization with sensor arrays," *IEEE Transactions on Signal Processing*, vol. 53, no. 8, pp. 3010–3022, 2005.

[30] J. Yin and T. Chen, "Direction-of-arrival estimation using a sparse representation of array covariance vectors," *IEEE Transactions on Signal Processing*, vol. 59, no. 9, pp. 4489–4493, 2011.

[31] W. Wang and H. Shao, "Range-angle localization of targets by a double-pulse frequency diverse array radar," *IEEE Journal of Selected Topics in Signal Processing*, vol. 8, no. 1, pp. 106–114, 2014.

[32] H. Wang, L. Wan, M. Dong, K. Ota, and X. Wang, "Assistant vehicle localization based on three collaborative base stations via SBL-based robust DOA estimation," *IEEE Internet of Things Journal*, vol. 6, no. 3, pp. 5766–5777, 2019.

[33] D. Meng, X. Wang, M. Huang, L. Wan, and B. Zhang, "Robust weighted subspace fitting for DOA estimation via block sparse recovery," *IEEE Communications Letters*, vol. 24, no. 3, pp. 563–567, 2020.

[34] X. Wang, L. Wan, M. Huang, C. Shen, Z. Han, and T. Zhu, "Low-complexity channel estimation for circular and noncircular signals in virtual MIMO vehicle communication systems," *IEEE Transactions on Vehicular Technology*, vol. 69, no. 4, pp. 3916–3928, 2020.

[35] P. Stoica and R. Moses, *Spectral Analysis of Signals*, Prentice Hall, 2005.